A Wearable Functional Near-Infrared Spectroscopy (fNIRS) System for Obstructive Sleep Apnea Assessment

Xude Huang, Jinbu Tang, Jingchun Luo, Feng Shu, Chen Chen, and Wei Chen, *Senior Member, IEEE*

***Abstract*— Obstructive sleep apnea (OSA), one of the most common sleep-related breathing disorders, contributes as a potentially life-threatening disease. In this paper, a wearable functional near-infrared spectroscopy (fNIRS) system for OSA monitoring is proposed. As a non-invasive system that can monitor oxygenation and cerebral hemodynamics, the proposed system is dedicated to mapping the pathogenic characteristics of OSA to dynamic changes in blood oxygen concentration and to constructing an automatic approach for assessing OSA. An algorithm including feature extraction, feature selection, and classification is proposed to signals. Permutation entropy(PE), for quantitative measuring the complexity of time series, is firstly involved to characterize the features of the physiological signals. Subsequently, the principal component analysis (PCA) for feature dimensionality reduction and support vector machine (SVM) algorithm for OSA classification are applied. The proposed method has been validated on a dataset that collected by the wearable system. It includes 40 subjects and composes of normal, and various severity cessation of breathing (e.g., mild, moderate, and severe). Experimental results exhibit that the proposed system can effectively distinguish OSA and non-OSA subjects, with an accuracy of 91.89%. The proposed system is expected to pave the novel perspective for OSA assessment in terms of cerebral hemodynamics.**

***Index Terms*— OSA, fNIRS, PE, PCA, SVM.**

I. Introduction

OBSTRUCTIVE sleep apnea syndrome is a common sleep-related respiratory disease in clinic. It is typically characterized by paroxysmal stenosis or even closure of the upper respiratory tract during sleep, and results in decreased cerebral oxygen saturation and intermittent hypoxia [1] and would further lead to a variety of concurrent diseases [2], [3]. At present, the gold standard in diagnosing OSA is polysomnography (PSG), which records electroencephalography (EEG), electrocardiography (ECG), electrooculography (EMG), respiratory state, etc. for comprehensive analysis of OSA. However, PSG test is not only expensive but also requires the participation of professional and technical personnel. In addition, the interpretation of PSG is also time-consuming and laborious. Thus, the clinical popularization and practicability of PSG may be limited in many medically underserved areas [4]. It is significant to explore a simple and accurate screening method to identify OSA.

Recently, the existing OSA assessment methods can be roughly divided into two categories: noncontact and contact approach. Noncontact approach is generally based on audio and video recording, etc. For example, OSA can be identified through snoring [5], speech [6], and vision-based cardiopulmonary signals [7]. Noncontact approach dramatically reduces the cost, but it is vulnerable to external environmental noise. Algorithms oriented toward eliminating the interference of noise need to be explored, which potentially increase the difficulty of the analysis algorithm. Besides, the accuracy of the OSA assessment may also be considerably impacted by these noises. In contrast, the contact approach focuses on assessing OSA via physiological signals collected by PSG or wearable devices, including single-lead ECG, respiratory flow, EEG, blood oxygen saturation, etc. [8], [9], [10], [11], [12], [13]. To illustrate, Sannino et al. used ECG to verify the possibility of ECG signal in OSA monitoring [11]. Kang et al. [12] and Abeyratne et al. [13] demonstrated significant differences in EEG between OSA and

Manuscript received 14 November 2022; revised 1 March 2023; accepted 17 March 2023. Date of publication 22 March 2023; date of current version 29 March 2023. This work was supported in part by the Shanghai Committee of Science and Technology under Grant 20S31903900, in part by the Shanghai Municipal Science and Technology International Research and Development Collaboration Project under Grant 20510710500, and in part by the National Natural Science Foundation of China under Grant 62001118. *(Corresponding authors: Chen Chen; Wei Chen.)*

This work involved human subjects or animals in its research. The authors confirm that all human/animal subject research procedures and protocols are exempt from review board approval.

Xude Huang is with the Center for Intelligent Medical Electronics, School of Information Science and Technology, Fudan University, Shanghai 200433, China (e-mail: 20210720261@fudan.edu.cn).

Jinbu Tang and Chen Chen are with the Human Phenome Institute, Fudan University, Shanghai 201203, China (e-mail: 21210880008@m.fudan.edu.cn; chenchen_fd@fudan.edu.cn).

Jingchun Luo is with the Human Phenome Institute, Zhangjiang Fudan International Innovation Center, Fudan University, Shanghai 201203, China (e-mail: luojc@fudan.edu.cn).

Feng Shu is with the Shanghai Engineering Research Center of Ultra-Precision Motion Control and Measurement, Academy for Engineering and Technology, Fudan University, Shanghai 200433, China (e-mail: fshu@fudan.edu.cn).

Wei Chen is with the Center for Intelligent Medical Electronics, School of Information Science and Technology, Fudan University, Shanghai 200433, China, and also with the Human Phenome Institute, Fudan University, Shanghai 201203, China (e-mail: w_chen@fudan.edu.cn).

Digital Object Identifier 10.1109/TNSRE.2023.3260303

non-OSA. Although favorable performance can be achieved by the contact approach, the physiological and psychological mechanisms under abnormal EEG/ECG activity in OSA patients is still unclear, and need to be further explored to verify the reliability of the proposed systems. In addition, most of the contact approach relies on the physiological signals collected by PSG. A wearable device that can take into account both high-precision real-time signal acquisition and accurate OSA identification is rare. Whether it is possible to combine the physiological mechanism of OSA and the actual signs and symptoms of OSA patients to develop a wearable OAS detection system still needs to be discussed.

In recent years, quantities of studies have shown that OSA can lead to instability of cerebral hemodynamics, and the blood oxygen concentration in the brain changes significantly during the occurrence of breathing obstruction [14], [15], [16]. Meanwhile, with the gradual improvement and maturity of functional near-infrared spectroscopy (fNIRS) technology, fNIRS provides a convenient and non-invasive method to detect changes in oxyhemoglobin and deoxygenated hemoglobin in brain tissue [17]. Although scattered literature has reported the possibility of applying fNIRS in sleep state evaluation, the utilization of fNIRS to assess OSA has never been explored. For example, Thien et al. [18] used fNIRS to study the spontaneous activity of the brain during sleep, and demonstrated the high feasibility of applying fNIRS to monitor oxyhemoglobin, deoxyhemoglobin, and total hemoglobin in the sleep phase. However, the feasibility of using dynamic changes in hemodynamic activity on the cerebral cortex for OSA assessment has not been mentioned.

Thus, combining the physiological mechanism of OSA, the actual signs and symptoms of OSA patients, and fNIRS technology, a wearable device for real-time monitoring of OSA based on fNIRS signals is proposed. The device can not only quickly and accurately detect changes in blood oxygen concentration on the cerebral cortex, but also has a low detection cost, and the detection environment has little binding force on the detection accuracy. Apart from designing a system to acquire fNIRS signals, an effective algorithm including feature extraction, feature selection, and classification is proposed to verify the feasibility of OSA assessment via cerebral hemodynamics. The main contributions of this paper are summarized as follows:

1): Different from the existing OSA detection schemes, a novel approach that combines the physiological mechanism of OSA, the clinical manifestations and characterizations of OSA, and fNIRS technology for OSA assessment is proposed.

2): To perceive and collect fNIRS signals more stably and reliably, a miniaturized fNIRS monitoring device is developed in this paper. The device is characterized by small volume and fast detection speed.

3): Based on the monitored fNIRS signals, the PE algorithm to extract discriminative features is proposed. The unique advantages of the PE algorithm are mainly reflected in: first, the calculation is simple and the anti-noise ability is strong; second, the algorithm is susceptible to time and can obtain higher resolution; third, the output results of the algorithm are intuitive and have better identification of mutation information.

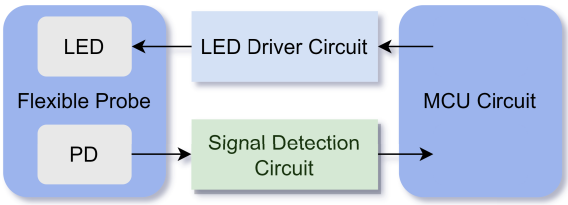

(a) Circuit System Block Diagram.

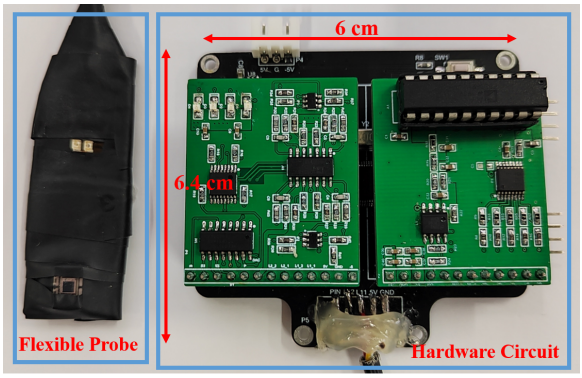

(b) Circuit System.

Fig. 1. Fig. 1(a) shows the block diagram of the circuit system. Fig. 1(b) is the prototype of the proposed system.

II. System Architectrue Design

The system framework is shown in Fig. 1(a). The whole system is divided into four subsystems: MCU circuit, LED drive circuit, signal detection circuit, and flexible probe. The MCU circuit controls the LED driver circuit. Photodetectors on the flexible probe detect the photons reflected by the tissue and convert them into voltage signals. The signal detection circuit extracts the weak voltage signal from the noise. The ADC on the MCU converts the analog voltage signal output by the signal detection circuit into a digital signal. The MCU uses the embedded algorithm to process the relevant digital signals and sends the processing results to the host computer through the serial port. Fig. 1(b) is the final circuit system.

A. Principles of the fNIRS System

For the main components in blood, fNIRS technology has good scattering properties in near-infrared light with wavelengths of 600-1000 nm. When the wavelength of light is about 800 nm [19], [20], [21], the absorbance of deoxyhemoglobin and oxyhemoglobin to light is equal; When the wavelength of light is less than 800 nm, the absorption rate of deoxyhemoglobin is greater than that of oxyhemoglobin; When the wavelength of light is greater than 800 nm, the absorption rate of light by oxyhemoglobin will exceed that of deoxyhemoglobin. Based on this effect, we can derive the amount of change in deoxyhemoglobin and oxyhemoglobin at a certain moment according to the modified Beer-Lambert law.

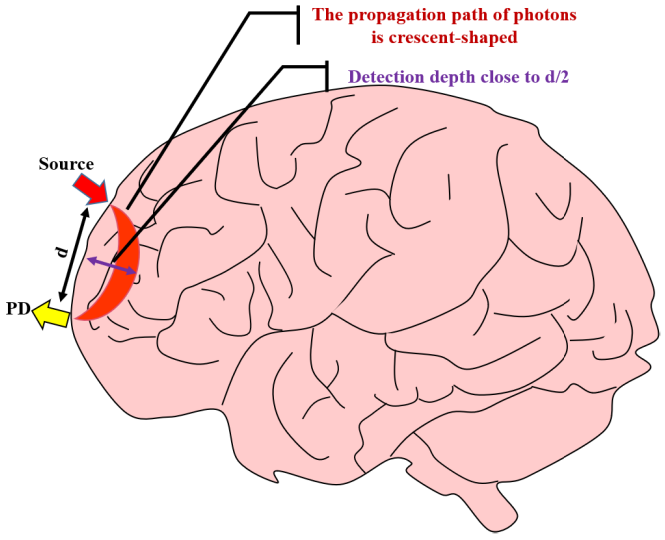

Fig. 2. Simple schematic diagram of fNIRS system.

The following formula is given in the paper [22]:

$$\begin{bmatrix}\Delta C_{HbO}\\ \Delta C_{HbR}\end{bmatrix} = \overline{M}^{-1} \times \overline{\Delta OD} = \overline{M}^{-1} \times \begin{bmatrix}\Delta OD^{\lambda_1}\\ \Delta OD^{\lambda_2}\end{bmatrix} \quad (1)$$

$$\Delta OD^{\lambda} = OD^{\lambda,t_1} - OD^{\lambda,t_2} \quad (2)$$

$$\overline{M} = d \cdot \left(\overline{\varepsilon} \times \overline{DPF}\right)^{T} \quad (3)$$

We can know that the concentration changes of deoxyhemoglobin (HbR) and oxyhemoglobin (HbO) are related to the optical density change matrix $\overline{\Delta OD}$ and the coefficient matrix $\overline{M}$, as in (1). The optical density variation matrix $\overline{\Delta OD}$ contains two different wavelengths of light. In the previous content, we discussed the absorption characteristics of two proteins at different wavelengths. In order to accurately measure the concentration changes of the two hemoglobins, we need to select one wavelength each in the front and back bands of 800 nm. In this paper, we choose two wavelengths, 760 nm and 850 nm. The coefficient matrix $\overline{M}$ is related to three parameters: d, $\overline{\varepsilon}$, $\overline{DPF}$.

1) d: Fig. 2 is a simple schematic diagram of the fNIRS system. The propagation path of photons in human tissue is crescent-shaped d represents the distance between the light source and the photodetector. It is mentioned in [23] that the detection depth of the NIR sensor is approximately $d/2$. The device proposed in this paper is used for brain forehead detection. The thickness of the human frontal bone is between 5 mm–10 mm. When d is 30 mm, the detection depth of the sensor is approximately 15 mm. At this detection depth, photons can pass through the frontal bone of the human body.

2) $\overline{\varepsilon}$: $\overline{\varepsilon}$ is the extinction coefficient matrix, its definition is given by (4):

$$\overline{\varepsilon} = \begin{bmatrix}\varepsilon_{HbO,\lambda_1} & \varepsilon_{HbO,\lambda_2}\\ \varepsilon_{HbR,\lambda_1} & \varepsilon_{HbR,\lambda_2}\end{bmatrix} \quad (4)$$

The extinction coefficient matrix is a constant matrix. The extinction coefficient reflects the absorption ability of the measured object to light, which is related to the wavelength of the light. In this paper, we take 760 nm and 850 nm as detection light wavelengths. Table I gives the extinction coefficient of deoxyhemoglobin and oxyhemoglobin at these two wavelengths.

TABLE I
CORRELATION EXTINCTION COEFFICIENT

nm	HbR	HbO
760	1.6745	0.6096
850	0.7861	1.1596

TABLE II
DIFFERENTIAL PATH LENGTH FACTOR

nm	DPF
760	6.2966
850	5.23433

3) DPF: $\overline{DPF}$ is the differential path length factor matrix, given by (5):

$$\overline{DPF} = \begin{bmatrix}DPF_{\lambda_1} & 0\\ 0 & DPF_{\lambda_2}\end{bmatrix} \quad (5)$$

The relevant calculation formula (6) is given in the literature [24]:

$$DPF(\lambda, A) = \alpha + \beta A^{\gamma} + \delta\lambda^3 + \varepsilon\lambda^2 + \zeta\lambda$$
$$\alpha = 223.3, \beta = 0.05624, \gamma = 0.8493$$
$$\delta = -5.723 \times 10^{-7}, \varepsilon = 0.001245, \zeta = -0.9025 \quad (6)$$

λ is the wavelength of light. A is age, and A is 30 in this paper. Based on (6) and related parameters, we calculated DPF values at 760 nm and 850 nm. In Table II, we list these values.

An fNIRS system is essentially an optical system, which consists of a light source and a photodetector. The system proposed in this paper needs to be placed on the forehead of the brain. In order to avoid irreversible damage to the human eye, we use LED as the light source. Although the fNIRS system is a noninvasive detection system, the LED light source in the system needs to be close to the skin. In the process of long-term detection, the temperature of the contact between the light source and the skin will gradually rise. When the temperature of the joint exceeds 41 degrees Celsius, the skin tissue of the human body will be damaged. Therefore, it is necessary to discuss the radiant energy of LED. It is mentioned in the article [25] that for coherent light sources in the range of 700 nm–1000 nm, the maximum permissible exposure (MPE) of skin is given by (7).

$$MPE = 2000 \cdot 10^{0.002(\lambda-700)}\left[W/m^2\right] \quad (7)$$

Using (7), we can calculate the MPE of coherent light sources at 760 nm and 850 nm (Table III), while the MPE of LED (incoherent) light sources at the same wavelength will be less than these values. The LEDs we use are 0805 SMD packages. The area of this package is $2.4mm^2$. Under the 0805 package, for the LED with wavelength of 760nm, we choose the power to be less than 6.3mW. For an 850 nm LED, this value cannot exceed 9.6mW. These discussions will guide us in the selection of LED devices.

TABLE III
MPE FOR 760NM AND 850NM COHERENT LIGHT SOURCES

nm	$MPE\ (mW/mm^2)$
760	2.64
850	3.99

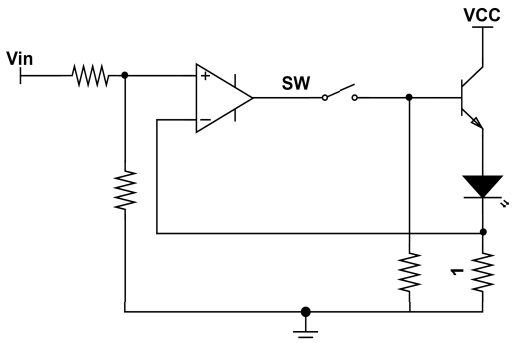

Fig. 3. Regulator of the LED current [27].

B. Circuit System Design

1) MCU Circuit: The core of the MCU circuit is an STM32f103c8t6 microcontroller. This microcontroller has peripherals such as 12-bit ADC, DMA, serial port, etc. In addition, it can generate PWM (Pulse Width Modulation) waves. In other experiments, ADCs with more than 10 bits have been shown to make reliable measurements. The highest frequency of STM32f103c8t6 microcontroller can reach 72MHZ. In the divide-by-six mode, it takes 21us for the ADC to get a conversion result. The paper [26] pointed out that the physiological signal of the forehead of the brain is in the range of 0-6HZ, which is a slowly changing signal. The fNIRS system proposed in this paper is mainly used for the detection of sleep apnea. From breathing obstruction to causing blood oxygen change, this is not a fast change process. Therefore, the ADC of the STM32f103c8t6 microcontroller meets the design requirements of our system.

2) LED Driver Circuit: In the fNIRS system, in order to accurately measure the transformation of physiological signals, the luminous intensity of the LED needs to be constant. The traditional LED driver circuit can be simplified as an ideal LED series connected with a current limiting resistor. Although this circuit is simple, over time, the current limiting resistor is heated and its resistance value will change. This causes the LED's light to be non constant. The LED driver circuit in this paper refers to an LED driver circuit proposed in [27]. In this circuit, the current flowing through the LED is related to the voltage across the 1 ohm resistor. The voltage across 1 ohm is positively related to the input voltage.

3) Signal Detection Circuit: The light signal reflected through the cerebral cortex is a very weak signal. In order to detect the target signal, this paper adopts the lock-in amplification technology. Weak voltage signals are easily submerged in various noises. The lock-in amplifier can extract the weak voltage signal from the noise and measure it accurately. The core of the lock-in amplifier is the phase-sensitive detection technology. It takes the reference signal that has the same frequency and fixed phase relationship with the signal to be measured as the reference, filters out the noise different from its frequency, and extracts the useful signal components.The principle of the lock-in amplifier circuit is shown in Fig. 4. The heart of the circuit is a phase sensitive detector. And the phase sensitive detector consists of a multiplier and a low pass filter. The input signal $S_{in}\,(t)$ and the reference signal $S_r\,(t)$ are as follows:

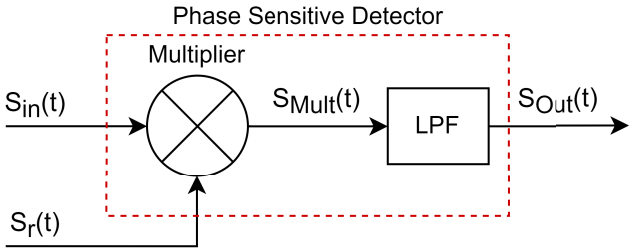

Fig. 4. The principle of the lock-in amplifier circuit.

$$S_{in(t)} = A\sin\left(wt + \varphi_{in}\right) + noise\,(t) \tag{8}$$

$$S_r\,(t) = B\sin\left(w_r t + \varphi_r\right) \tag{9}$$

$noise\,(t)$ includes ambient noise and noise introduced by the circuit before the lock-in amplifier circuit. After going through the multiplier, we can get $S_{Mult}\,(t)$:

$$\begin{aligned} S_{Mult}\,(t) =& 0.5AB\cos\left(\left(w - w_r\right)t + \varphi_{in} - \varphi_r\right) \\ &- 0.5AB\cos\left(\left(w + w_r\right)t + \varphi_{in} + \varphi_r\right) \\ &+ Bnoise\,(t)\sin\left(w_r t + \varphi_r\right) \end{aligned} \tag{10}$$

When $w = w_r$, $S_{Mult}\,(t)$ can be simplified to

$$\begin{aligned} S_{Mult}\,(t) =& 0.5AB\cos\left(\varphi_{in} - \varphi_r\right) \\ &- 0.5AB\cos\left(2w_r t + \varphi_{in} + \varphi_r\right) \\ &+ Bnoise\,(t)\sin\left(w_r t + \varphi_r\right) \end{aligned} \tag{11}$$

In (11), $0.5AB\cos\left(\varphi_{in} - \varphi_r\right)$ is a constant term. When w_r is a very high value, the remaining two terms in (11) become high frequency terms. In this paper, we set the cutoff frequency of the low-pass filter to 3 Hz and use a 4th-order Butterworth low-pass filter. After filtering out by a low-pass filter, we get:

$$S_{Out}\,(t) = 0.5AB\cos\left(\varphi_{in} - \varphi_r\right) \tag{12}$$

When the reference signal and the input signal have the same phase, i.e., $\varphi_{in} = \varphi_r$:

$$S_{Out}\,(t) = 0.5AB \tag{13}$$

We can know from the output signal: the output of the lock-in amplifier is a DC voltage, which is proportional to the signal amplitude of a specific frequency (the frequency consistent with the reference signal frequency) in the input signal. In this article, we use ADI's AD630 chip to build a lock-in amplifier circuit. The reference signal required in the lock-in amplifier circuit is consistent with the PWM wave in the LED driver circuit. In this way, we can achieve accurate detection of a certain frequency signal.

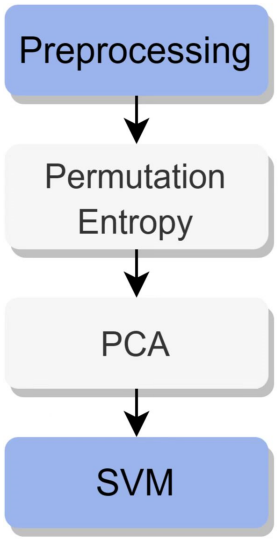

Fig. 5. Algorithm Flowchart.

4) Flexible Probe: A dual-wavelength LED and a photodetector chip are integrated on the flexible probe. The fNIRS system proposed in this paper is mainly used for brain forehead measurements. Through the analysis above, the distance between the light source and the photodetector is 3 cm. A person's forehead has a certain arc. If the probe adopts a rigid circuit board, it will cause the problem that the light source or photoelectric detector cannot be closely attached to the head. To solve this problem, we use a flexible printed circuit (FPC) to design the probe. fNIRS systems are susceptible to internal light pollution (ILP). ILP refers to the fact that the light emitted by the LED is directly received by the photodetector and does not contain any physiological information. In order to solve this problem, we need to do light isolation between the LED and the photodetector. In this paper, black tape is used to block light.

III. Methods

In this section, the experimental protocol for verifying the feasibility of the proposed system is presented, followed by the specific flow of the proposed algorithm, as shown in Fig.5. First, the preprocessing module will remove outlier points and baselines from the signal while normalizing the signal. Next, informative features are extracted by permutation, and feature dimension reduction is performed by PCA. Finally, the features are fed into SVM, and the predicted label of data, including non-OSA and OSA, can be obtained.

A. Experimental Procedure

To verify the effectiveness of the device in sleep breathing monitoring, we designed a sleep apnea simulation experiment. In this experiment, a total of 40 healthy subjects, including 20 males and 20 females were recruited. The whole experimental process strictly abides by the relevant experimental guidelines. Each subject was fully informed of the risks involved in the experimental process and was asked to sign an informed consent before the experiment. The experiment was carried out in a softly lit room. The temperature of the whole room is around 20°C, and the humidity is kept at 50%RH. The experimental is conducted at 13:00-17:00 for all the subjects. Before the start of the experiment, we will use medical alcohol cotton to clean the subject's forehead, and then use medical tape to fix the probe. During the experiment, we asked each subject to close their eyes and remain still. After the experiment guide gave instructions, the subjects began to hold their breath or breathe normally.

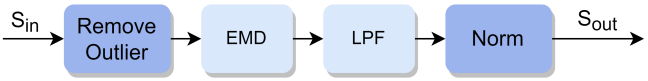

Fig. 6. Data Preprocessing.

According to the guidelines proposed by American Academy of Sleep Medicine (AASM), sleep apnea can be divided into 4 grades: normal, mild, moderate, and severe. Normal, AHI: 0–5 times/h; mild, AHI: 5–15 times/h; moderate, AHI: 15–30 times/h; severe, AHI≥30 times/h (Sleep Apnea Hypopnea Index, AHI). We divided 40 healthy subjects into 4 groups, each consisting of 5 women and 5 men. And the experiment time for each subject is one hour.

We make the following arrangements for the four groups:

1) The subjects in the normal group lie down peacefully for an hour without any intervention.
2) The subjects in the mild group held breath-holding every 6 minutes, and the duration of each breath-holding was 20s, a total of 9 times.
3) The subjects in the moderate group held their breath randomly 20 times, and the duration of breath-holding of 15 seconds, 16 seconds and 20 seconds appeared randomly.
4) Subjects in the severe group held their breath for 32 times at random, and the duration of breath-holding of 15 seconds, 16 seconds and 20 seconds appeared randomly.

B. Preprocessing

A total of 40 subjects were recruited for the experiment. Because the probe of 3 subjects was loose during the experiment and no valid data was collected, we obtained 37 valid data. We preprocess the valid data following the procedure shown in Fig.6. Firstly, outliers caused due to some unexpected factors (such as sneezing) during the experiment were removed. Afterward, an empirical mode decomposition (EMD) algorithm to remove motion artifacts is applied. EMD is to decompose the signal according to the time scale characteristics of the data itself, without any pre-set basis functions. Therefore, the EMD method can stabilize the non-stationary data and improve the signal-to-noise ratio when dealing with non-stationary and nonlinear data. Then, a digital low-pass filter (LPF) dedicated to leaking physiological signals in specific frequency bands is used. Finally, the data is normalized.

When the subjects hold their breath according to the experimental paradigm, the signal will show a downward trend; when the subjects relax, the signal will rise. Therefore, there is a trough in the time domain when the event occurs. We use the

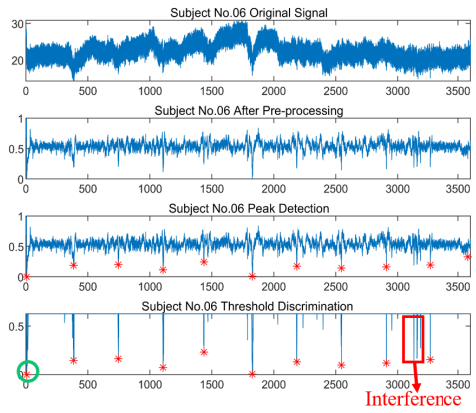

(a) Results of mild Subject No.06. The target event occurs 9 times. 10 times are actually obtained, 9 times are valid, and 1 time is falsely detected (at the green circle).

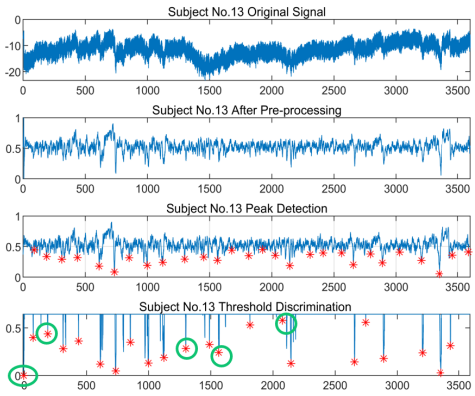

(b) Results of moderate Subject No.13. Target event occurs 20 times. 22 times are actually obtained, 17 times are valid, and 5 times are falsely detected (the green circle).

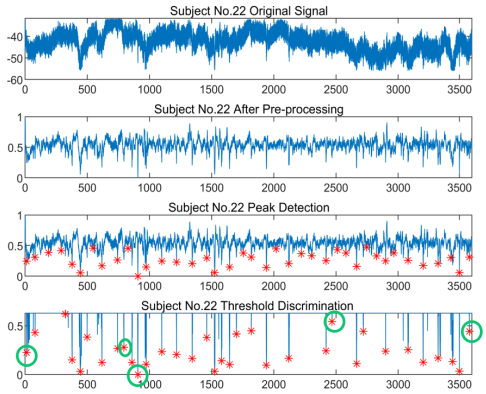

(c) Results of severe Subject No.22. The target event occurs 32 times. 34 times are actually obtained, 29 times are valid, and 5 times are falsely detected (the green circle)

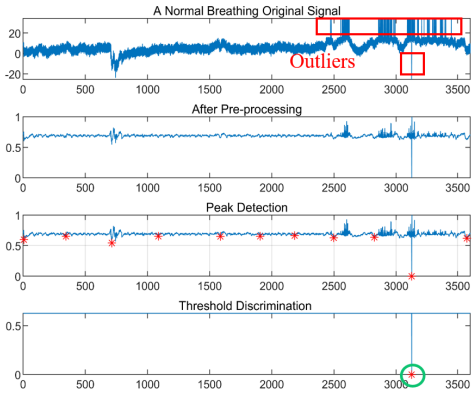

(d) The figure shows the data of a subject with normal breathing. The raw data contains many outliers (red box). Our algorithm can remove many outliers. However, some of the remaining outliers will still affect the detection results. As the figure shows, the normally breathing subject did not hold his breath. But due to outlier interference, our device detected an error event (circled in green).

Fig. 7. The preprocessing results of the experimental data of the four subjects. Fig. 7(a) shows the data of a female subject with mild breath-holding. Fig. 7(b) shows the data of a male subject with moderate breath-holding. Fig. 7(c) shows the data of a female subject with severe breath-holding. Fig. 7(d) is the data of a female subject with normal breathing.

peak detection function and threshold discriminant function that comes with MATLAB to detect the troughs in the signal. In the threshold discrimination, we first calculate the standard deviation of S_{out}, and then use 6.5–9 times this standard deviation as the threshold.Fig. 7(a) is the experimental result of a mild subject(ID: Subject No.06); Fig. 7(b) is the experimental result of a moderate subject(ID: Subject No.13); Fig. 7(c) is the experimental result of a severe subject(ID: Subject No.22); Fig. 7(d) is the experimental result of a normal subject.In Fig. 7(a), comparing the mild experimental paradigm, we can find that there is a misjudgment (green circle) in the final threshold discrimination result. The main reason for this misjudgment is the existence of unavoidable interference. This interference mainly comes from two aspects:

1) The disturbance when the circuit system is powered on.
2) The physiological activity of the human body in the interval between the experimental events.

No matter where it comes from, this disturbance will inevitably affect the final result of the experiment. Many outliers appear as shown in Fig. 7D. These outliers higher/lower than the threshold are removed for reducing system errors. However, there are still some outliers that have not been removed. This leads to an error in the final threshold discrimination result.

C. Feature Extraction and Reduction

In this paper, we use the PE algorithm to obtain features of time-domain signals. PE is a measure of the complexity of a time series. It introduces the idea of PE when calculating the complexity between reconstructed subsequences. The PE algorithm was proposed by Bandt and Pompe in 2002 [28].

The basic principle of the algorithm is as follows (formula reference [29]):

1) For a digital signal $X = \{x_1, x_2, x_3 \ldots x_n\}$, its length is n. We set the length of the subsequence to m and

the time delay parameter to τ, and we can get k subsequences, as show in (14), $k = n - (m-1)\tau$.

$$\begin{gathered}\left\{x_1, x_{1+\tau}, \ldots, x_{1+(m-1)\tau}\right\}\langle 1\rangle \\ \left\{x_2, x_{2+\tau}, \ldots, x_{2+(m-1)\tau}\right\}\langle 2\rangle \\ \cdots \\ \left\{x_k, x_{k+\tau}, \ldots, x_{k+(m-1)\tau}\right\}\langle k\rangle\end{gathered} \tag{14}$$

2) The element in each subsequence consists of two parts: one is the size of the element value, and the other is the position label of the element. For example, for a sequence $\{4, 6, 5\}$, the value of the first element is 4, and the position number of the first element is 1. The position number of each element in the subsequence can also form a sequence. For sequence $\{4, 6, 5\}$, the sequence formed by the position number of each element is $\{1, 2, 3\}$. For a subsequence with a length of m, the sequence composed of position labels is $\{1, 2, \ldots, m\}$. Define index sequence$S(\iota)$, the k subsequences have the following expression.

$$\begin{gathered}S(\iota) = \{1, 2, \ldots, m\} \\ \iota = 1, 2, \cdots, k\end{gathered} \tag{15}$$

3) Let's take the sequence $\{4, 6, 5\}$ as an example. The sequence formed by the element index is $\{1, 2, 3\}$. The sequence $\{4, 6, 5\}$ is sorted in ascending order to obtain the sequence $\{4, 5, 6\}$, and the index sequence is also moved to obtain the sequence $\{1, 3, 2\}$. For k subsequences, k new index sequences can be obtained. In the k new index sequences, we can calculate the probability of occurrence of each different sequence, defined as P. According to the Shannon entropy, the calculation formula of Permutation Entropy can be obtained (16).

$$H_p = -\sum_{j=1}^{j\leq k} P_j \ln P_j \tag{16}$$

4) For the sequence with length of m, there are $m!$ possible permutations. Normalize H_p:

$$H_p = -\frac{1}{\ln(m!)} \sum_{j=1}^{j\leq k} P_j \ln P_j \tag{17}$$

After the calculation of the PE algorithm, a feature matrix of 37*35575 is obtained. There are only 37 valid samples in total. But the feature count per sample is 35575. We found that the number of features is much larger than the number of samples. The number of features is very large and contains a lot of noise. Considering that if we directly classify without dimensionality reduction, it is very likely that the model will be difficult to converge. This will affect the classification accuracy. Thus, the PCA algorithm is used for data dimensionality reduction. After the dataset is reduced by PCA, the dimension size becomes 37*36.

D. Support Vector Machines (SVM)

In this paper, SVM is adopted for classification. The goal of SVM is to make the distance between various sample points and the hyperplane the furthest, that is, to find the maximum interval hyperplane. Any hyperplane can be described by the linear equation $w^T x + b = 0$. We can deduce the optimization problem of SVM according to the related theory of SVM:

$$min\frac{1}{2}\|w\|^2 \, s.t. y_i\left(w^T x_i + b\right) \geq 1 \tag{18}$$

Constructing the Lagrangian function:

$$\begin{gathered}\min_{w,b}\max_{\lambda} L = \frac{1}{2}\|w\|^2 + \sum_{i=1}^{n}\lambda_i\left[1 - y_i\left(w^T x_i + b\right)\right] \\ s.t.\ \lambda_i \geq 0\end{gathered} \tag{19}$$

Using strong duality transformations:

$$\max_{\lambda}\min_{w,b} L(w, b, \lambda) \tag{20}$$

Find partial derivatives for parameters w, b:

$$\begin{cases}\dfrac{\partial L}{\partial w} = w - \sum_{i=1}^{n}\lambda_i x_i y_i = 0 \\ \dfrac{\partial L}{\partial b} = \sum_{i=1}^{n}\lambda_i y_i = 0\end{cases} \tag{21}$$

Bring $\frac{\partial L}{\partial w}, \frac{\partial L}{\partial b}$ into $L(w, b, \lambda)$ to get:

$$\min_{w,b} L(w, b, \lambda) = \sum_{i=1}^{n}\lambda_i - \frac{1}{2}\sum_{i=1}^{n}\sum_{j=1}^{n}\lambda_i\lambda_j y_i y_j\left(x_i \cdot x_j\right) \tag{22}$$

Then it can be obtained:

$$\begin{gathered}\max_{\lambda} \sum_{i=1}^{n}\lambda_i - \frac{1}{2}\sum_{i=1}^{n}\sum_{j=1}^{n}\lambda_i\lambda_j y_i y_j\left(x_i \cdot x_j\right) \\ s.t. \sum_{i=1}^{n}\lambda_i y_i = 0, \lambda_i \geq 0\end{gathered} \tag{23}$$

We can obtain the optimal λ through the SMO (Sequential Minimal Optimization) algorithm. Bringing λ into $\frac{\partial L}{\partial w}$ gives w, and then b. When we obtain w, b we can construct the maximum segmentation hyperplane: $w^T x + b = 0$.

E. Performance Evaluation

In this paper, we use the leave-one-out cross-validation method for performance evaluation. In leave-one-out cross-validation, we take a set of data set D as a validation set each time until all samples have been used as a validation set. This process is calculated N times in total, we average the validation errors, and finally obtain the accuracy (Acc). The size of N is related to categorical events. We obtained available data for a total of 37 cases. Among them, 10 were mild, 10 were moderate, 7 were severe, and 10 were normal. If all available samples are classified with and without OSA, then N = 37. If we classify normal breathing samples and severe breath hold samples, then N = 17.

TABLE IV
MILD(DEGREE=9), MODERATE(DEGREE=20), SEVERE(DEGREE=32) EXPERIMENTAL DATA

Subject	Gender	Degree	Measured times	FP	TP	Recall	Precision	F_1
Subject1	Male	9	9	2	7	77.78%	77.78%	0.78
Subject2	Male	9	10	3	7	77.78%	70.00%	0.74
Subject3	Male	9	10	1	9	100.00%	90.00%	0.95
Subject4	Male	9	6	2	4	44.44%	66.67%	0.53
Subject5	Male	9	10	4	6	66.67%	60.00%	0.63
Subject6	Female	9	10	1	9	100.00%	90.00%	0.95
Subject7	Female	9	11	4	7	77.78%	63.64%	0.70
Subject8	Female	9	10	6	4	44.44%	40.00%	0.42
Subject9	Female	9	6	0	6	66.67%	100.00%	0.80
Subject10	Female	9	8	3	5	55.56%	62.50%	0.59
Mean(mild)						71.11%	72.06%	0.71
Subject11	Male	20	30	14	16	80.00%	53.33%	0.64
Subject12	Male	20	22	12	10	50.00%	45.45%	0.48
Subject13	Male	20	22	5	17	85.00%	77.27%	0.81
Subject14	Male	20	35	20	15	75.00%	42.86%	0.55
Subject15	Male	20	28	16	12	60.00%	42.86%	0.50
Subject16	Female	20	21	8	13	65.00%	61.90%	0.63
Subject17	Female	20	30	18	12	60.00%	40.00%	0.48
Subject18	Female	20	31	17	14	70.00%	45.16%	0.55
Subject19	Female	20	33	22	11	55.00%	33.33%	0.42
Subject20	Female	20	25	12	13	65.00%	52.00%	0.58
Mean(moderate)						66.50%	49.42%	0.56
Subject21	Male	32	38	12	26	81.25%	68.42%	0.74
Subject22	Male	32	34	5	29	90.63%	85.29%	0.88
Subject23	Male	32	33	10	23	71.88%	69.70%	0.71
Subject24	Male	32	33	17	16	50.00%	48.48%	0.49
Subject25	Female	32	37	16	21	65.63%	56.76%	0.61
Subject26	Female	32	34	17	17	53.13%	50.00%	0.52
Subject27	Female	32	36	18	18	56.25%	50.00%	0.53
Mean(severe)						66.96%	61.24%	0.64

IV. RESULTS

A. Statistical Analysis

In this article, we define Precision as the ratio of the number of True Positive (TP) to the total measured times. We also define the Recall as the ratio of the number of correct detections to the actual number of breath holdings ($Degree$). For example, in Fig. 7(a), after threshold, we detected 10 times (10 red dots, Measured times $= 10$), of which 9 were detected correctly ($TP = 9$), and one was detected incorrectly (False Positive, $FP = 1$). Because Subject No.06 participated in the mild simulation experiment, her actual number of breath holdings was 9 ($Degree = 9$). In addition, F_1 which balances the precision and recall is also used. When F_1 is high, it indicates that the test method is more effective.

$$Precision = \frac{TP}{FP + TP} \tag{24}$$

$$Recall = \frac{TP}{Degree} \tag{25}$$

$$F_1 = 2 \cdot \frac{Precision \cdot Recall}{Precision + Recal} \tag{26}$$

In Table IV, we list the statistics of event detection for all subjects. We give the average value of each indicator(precision, recall, F_1)at different levels(mild, moderate, severe). According to Table IV, we find that our device performs best in mild experiments. The average recall of the mild experiment reached 71.11%, and the average precision reached 72.06%. In the moderate and severe experiments, the average recalls of the two are very close, which are 66.5% and 66.96%, respectively. For the average precision, the data from the severe experiment performed better. The average precision of the severe experiment was 61.24%, while the average precision of the moderate experiment was only 49.42%. In mild experiments, subjects periodically held their breath. In terms of scenarios, the mild experiment is closer to the state of the patient's onset. In the mild experiment, both the recall and precision have reached the standard of primary screening of cases (>=70%). In the severe and moderate experiments, subjects held their breath at random. In this extreme scenario, the recall of the device also reached more than 65%. These results show that the robustness of our device is high.

TABLE V
CLASSIFICATION EVENTS AND ACCURACY WITH PCA

Event	Accuracy (Acc) with PCA
OSA VS No OSA	91.89%
mild VS moderate VS severe	70.37%
normal,mild VS moderate,severe	81.08%
normal,mild VS severe	81.48%
normal VS mild	75%
normal VS moderate	75%
normal VS severe	70.59%

B. Classification Results

We classify the obtained data using the proposed classification algorithm. We use PE to extract signal features, use PCA to reduce the dimensionality of the feature data and perform simple classification with SVM. The classification results are shown in Table V. From the results in Table V, we can find that the classification accuracy of the two types of signals of normal and abnormal breathing can reach 91.89%, which has

TABLE VI
CLASSIFICATION EVENTS AND ACCURACY WITH PCA OR WITHOUT PCA

Event	Acc with PCA	time	Acc without PCA	time
OSA VS No OSA	91.89%	0.25s	86.49%	6.28s
mild VS moderate VS severe	70.37%	0.21s	70.37%	5.08s
normal,mild VS moderate,severe	81.08%	0.38s	81.08%	7.5s
normal,mild VS severe	81.48%	0.29s	81.48%	2.81s
normal VS mild	75%	0.27s	40%	2.09s
normal VS moderate	75%	0.25s	75%	2.39s
normal VS severe	70.59%	0.21s	70.59%	1.60s

exceeded the criteria for primary screening of cases (>=70%). At the same time, the accuracy in distinguishing between severe and normal can reach 70.59%. What is more interesting is that the data for mild breath-holding and moderate breath-holding are more distinguishable from the data for normal breathing, and they are both 75%. In Table V, we found that the accuracy of classifying severe, moderate, and mild at the same time is 70.37%. It can also be seen from the results in Table V that our proposed classification method is more suitable for the determination of the presence or absence of disease (Acc=91.89%).

V. DISCUSSION

In this article, according to the relevant principles of fNIRS, the physiological mechanism and the clinical manifestations of OSA, a portable system for OSA monitoring is proposed. In the circuit design, the calculation process of the system parameters is described and provided. Given that fNIRS is an optical system, how to choose a suitable LED light source is presented. AD630 chip to build a lock-in amplifier circuit for signal detection is used. At the same time, we refer to the LED driver circuit of other articles in the text to provide a constant LED light source for the system. Since the forehead has a certain curvature, we integrated the LED and photoelectric conversion chip on a flexible circuit board to obtain a flexible probe.

Through the simulated apnea experiment, we collected 37 sets of data. Through the analysis and statistics of these data, we verified the feasibility of our system. In order to distinguish different levels of apnea samples, we propose a practical classification algorithm. We firstly applied the PE algorithm to extract features from the data and used PCA for dimensionality reduction. In addition, the SVM to roughly classify the data was applied. In Table VI, we compared the classification accuracy with and without PCA dimensionality reduction. Experimental results exhibited that the accuracy improved in most cases after PCA dimensionality reduction. In Table VII, we compared with existing research works [6], [30], [31]. In the paper [6], the authors used speech signal processing techniques to estimate the AHI in the awake state using linear regression. The average accuracy of this method is 77.14%. In the paper [30], the authors propose to use Domain Adversarial Neural Networks (DANN) to generate an OSA speech model. The accuracy of the model for severe OSA was 76.6%. In the paper [31], the authors utilize wireless tracheal audio sensors to measure audio data. The authors used AHI = 15 as the boundary condition for severe OSA and obtained 86% accuracy.By comparison, we find that our method shows

TABLE VII
COMPARISON WITH EXISTING WORKS

Events	Paper	ACC
OSA VS No OSA	[26] R.M.Simply et al.,2020	77.14%
	Our	**91.89%**
normal,mild VS severe	[27] J.M.Perero-Codosero et al.,2020	76.60%
	Our	**81.48%**
normal,mild VS moderate,severe	[28] M.MŁYŃCZAK et al.,2020	86%
	Our	**81.08%**

TABLE VIII
COMPARISON WITH OTHER MACHINE LEARNING METHODS

Classified Events	SVM	KNN	DecisionTree
OSA VS No OSA	**91.89%**	72.97%	71.17%
normal/mild VS severe	**81.48%**	74.07%	72.84%
normal/mild VS moderate /severe	**81.08%**	56.76%	53.15%

better performance in the two classes of scenarios. In the third type of scene (normal,mild VS moderate,severe), our classification method also achieves 81.08% accuracy. This also shows that the PE combined with SVM is feasible for OSA data classification. Considering the simplicity of the PE algorithm, we can deploy the algorithm directly to the MCU for real-time classification in the future.

In the field of OSA monitoring, our devices are small and inexpensive compared to traditional PSG devices. Our equipment is more competitive in the household field. Compared with means such as snoring monitoring, our device does not involve risks such as ethics, privacy and so on. In terms of feature extraction, PE is a measure of signal space complexity, which is simple and fast to calculate, and can better correlate nonlinear and non-stationary signals. Therefore, PE has good applicability. In Table VIII, we also compared our method with other traditional machine learning methods including KNN, Decision Tree. Taking OSA and No OSA as an example, KNN achieved 72.97% and Decision Tree achieved 71.17%. But the SVM can reach 91.89%. In the event normal/mild VS moderate/severe, the accuracy of the three classification methods has decreased, but the SVM still reaches 81.08%.

To our best knowledge, this is the first work to propose a wearable system that combines the physiological mechanism of OSA, the clinical manifestations of OSA, and fNIRS technique for OSA assessment. As a preliminary study, the feasibility is verified by a comprehensive protocol and experimental results reveal the effectiveness of the proposed system in OSA detection. However, there are still some issues that need to

be further explored. As a wearable optical system, motion artifacts are a big challenge. These motion artifacts may not only submerge original fNIRS signals but also increase the difficlutis in pre-processing. In the future, a three-axis acceleration to indicate the occurrence of motion will be involved. Secondly, currently, we only verified the feasibility of the proposed system on 37 subjects via an experimental protocol. The reliability of the proposed system can be validated by involving more subjects in a practical scenario.

VI. Conclusion

In this paper, a circuit for OSA monitoring is designed based on the principle of fNIRS by considering the physiological mechanism and the clinical manifestations of OSA. Meanwhile, an algorithm based on the obtained fNIRS signal for OSA assessment is proposed. It includes discriminative feature extraction via PE, feature dimensionality reduction using principal component analysis, and a classifier based on a support vector machine. To our best knowledge, it is the first work to explore the feasibility of OSA assessment via fNIRS, and the experimental results demonstrate that our system can reach excellent performance in judging the presence or absence of OSA. The proposed system not only exhibits great potential for home OSA monitoring via characterizing dynamic changes in blood oxygen concentration, but also offers an effective solution for quantifying the distinctions among healthy subjects and OSA subjects with different severities. In addition, we can deploy the proposed algorithm in the circuit system to achieve an online OSA assessment in the future.

References

[1] A. Culebras, "Are patients with obstructive sleep apnea at an increased risk of stroke or death?" *Nature Clin. Pract. Neurol.*, vol. 2, no. 6, pp. 306–307, Jun. 2006.

[2] C. Xu et al., "Lipoprotein-associated phospholipase A2 predicted cardiovascular disease in obstructive sleep apnea syndrome," *Respiratory Med.*, vol. 163, Mar. 2020, Art. no. 105881.

[3] U. Bicer, R. Kutlu, S. Yosunkaya, and I. Kilinc, "Evaluation of plasma ghrelin, omentin-1 levels and insulin resistance in patients with obstructive sleep apnea syndrome," *Konuralp Tip Dergisi*, vol. 13, pp. 114–121, Jan. 2021.

[4] G. Surrel, A. Aminifar, F. Rincón, S. Murali, and D. Atienza, "Online obstructive sleep apnea detection on medical wearable sensors," *IEEE Trans. Biomed. Circuits Syst.*, vol. 12, no. 4, pp. 762–773, Aug. 2018.

[5] P. Temrat, Y. Jiraraksopakun, A. Bhatranand, and K. Wea-Asae, "Suitable feature selection for OSA classification based on snoring sounds," in *Proc. 15th Int. Conf. Electr. Eng./Electron., Comput., Telecommun. Inf. Technol. (ECTI-CON)*, Jul. 2018, pp. 1–4.

[6] R. M. Simply, E. Dafna, and Y. Zigel, "Diagnosis of obstructive sleep apnea using speech signals from awake subjects," *IEEE J. Sel. Topics Signal Process.*, vol. 14, no. 2, pp. 251–260, Feb. 2020.

[7] M. H. Li, A. Yadollahi, and B. Taati, "Noncontact vision-based cardiopulmonary monitoring in different sleeping positions," *IEEE J. Biomed. Health Inform.*, vol. 21, no. 5, pp. 1367–1375, Sep. 2017.

[8] W. J. Da, H. H. Su, J. L. Yu, D. U. Jeong, and K. S. Park, "Apnea–hypopnea index prediction using electrocardiogram acquired during the sleep-onset period," *IEEE Trans. Biomed. Eng.*, vol. 64, no. 2, pp. 295–301, Feb. 2017.

[9] Z. Cao, R. Zhu, and R. Y. Que, "A wireless portable system with microsensors for monitoring respiratory diseases," *IEEE Trans. Biomed. Eng.*, vol. 59, no. 11, pp. 3110–3116, Nov. 2012.

[10] W. S. Almuhammadi, K. A. I. Aboalayon, and M. Faezipour, "Efficient obstructive sleep apnea classification based on EEG signals," in *Proc. Long Island Syst., Appl. Technol.*, May 2015, pp. 1–6.

[11] G. Sannino, I. De Falco, and G. De Pietro, "An automatic rules extraction approach to support OSA events detection in an mhealth system," *IEEE J. Biomed. Health Informat.*, vol. 18, no. 5, pp. 1518–1524, Sep. 2014.

[12] J. M. Kang, S.-E. Cho, K.-S. Na, and S.-G. Kang, "Spectral power analysis of sleep electroencephalography in subjects with different severities of obstructive sleep apnea and healthy controls," *Nature Sci. Sleep*, vol. 13, pp. 477–486, Apr. 2021.

[13] U. R. Abeyratne, V. Swarnkar, C. Hukins, and B. Duce, "Interhemispheric asynchrony correlates with severity of respiratory disturbance index in patients with sleep apnea," *IEEE Trans. Biomed. Eng.*, vol. 57, no. 12, pp. 2947–2955, Dec. 2010.

[14] R. M. Alex, N. D. Mousavi, R. Zhang, R. J. Gatchel, and K. Behbehani, "Obstructive sleep apnea: Brain hemodynamics, structure, and function," *J. Appl. Biobehavioral Res.*, vol. 22, no. 4, Dec. 2017, Art. no. e12101.

[15] Y. Xia, Y. Fu, H. Xu, J. Guan, H. Yi, and S. Yin, "Changes in cerebral metabolites in obstructive sleep apnea: A systemic review and meta-analysis," *Sci. Rep.*, vol. 6, no. 1, p. 28712, Jun. 2016.

[16] A. E. Beaudin, X. Waltz, P. J. Hanly, and M. J. Poulin, "Impact of obstructive sleep apnoea and intermittent hypoxia on cardiovascular and cerebrovascular regulation," *Exp. Physiol.*, vol. 102, no. 7, pp. 743–763, Jul. 2017.

[17] T. Hoshino, S. Kanoga, A. Kanemura, and T. Ogawa, "A no-reference metric of cerebral blood flow extraction for fNIRS data," in *Proc. IEEE Int. Conf. Syst., Man, Cybern. (SMC)*, Oct. 2018, pp. 83–89.

[18] T. Nguyen, O. Babawale, T. Kim, H. J. Jo, H. Liu, and J. G. Kim, "Exploring brain functional connectivity in rest and sleep states: A fNIRS study," *Sci. Rep.*, vol. 8, no. 1, p. 16144, Nov. 2018.

[19] S. Wray, M. Cope, D. T. Delpy, J. S. Wyatt, and E. O. R. Reynolds, "Characterization of the near infrared absorption spectra of cytochrome aa_3 and haemoglobin for the non-invasive monitoring of cerebral oxygenation," *Biochim. et Biophys. Acta (BBA)–Bioenergetics*, vol. 933, no. 1, pp. 184–192, 1988.

[20] A. Bakker, B. Smith, P. Ainslie, and K. Smith, "Near-infrared spectroscopy," in *Applied Aspects of Ultrasonography in Humans*, P. Ainslie, Ed. Rijeka, Croatia: InTech, 2012. [Online]. Available: http://www.intechopen.com/books/applied-aspects-of-ultrasonography-in-humans/near-infrared-spectroscopy

[21] F. Scholkmann et al., "A review on continuous wave functional near-infrared spectroscopy and imaging instrumentation and methodology," *NeuroImage*, vol. 85, pp. 6–27, Jan. 2014.

[22] A. Bozkurt, A. Rosen, H. Rosen, and B. Onaral, "A portable near infrared spectroscopy system for bedside monitoring of newborn brain," *Biomed. Eng. Online*, vol. 4, no. 1, pp. 1-11, 2005.

[23] G. Strangman, D. Boas, and J. Sutton, "Non-invasive neuroimaging using near-infrared light," *Biol. Psychiatry*, vol. 52, pp. 679–693, Nov. 2002.

[24] F. Scholkmann and M. Wolf, "General equation for the differential pathlength factor of the frontal human head depending on wavelength and age," *J. Biomed. Opt.*, vol. 18, no. 10, Oct. 2013, Art. no. 105004.

[25] C. J. Soraghan, T. E. Ward, F. Matthews, and C. Markham, "Optical safety assessment of a near-infrared brain–computer interface," in *Proc. IET Irish Signals Syst. Conf. (ISSC)*, 2008, pp. 174–179.

[26] A. Y. Rwei et al., "A wireless, skin-interfaced biosensor for cerebral hemodynamic monitoring in pediatric care," *Proc. Nat. Acad. Sci. USA*, vol. 117, no. 50, pp. 31674–31684, 2020.

[27] F. Chenier and M. Sawan, "A new brain imaging device based on fNIRS," in *Proc. IEEE Biomed. Circuits Syst. Conf.*, Nov. 2007, pp. 1–4.

[28] C. Bandt and B. Pompe, "Permutation entropy: A natural complexity measure for time series," *Phys. Rev. Lett.*, vol. 88, no. 17, Apr. 2002, Art. no. 174102.

[29] S. Ye, "Application and development of permutation entropy algorithm," *J. Acad. Armored Force Eng.*, vol. 26, no. 2, pp. 34–38, 2012.

[30] J. M. Perero-Codosero, F. Espinoza-Cuadros, J. Anton-Martin, M. A. Barbero-Alvarez, and L. A. Hernandez-Gomez, "Modeling obstructive sleep apnea voices using deep neural network embeddings and domain-adversarial training," *IEEE J. Sel. Topics Signal Process.*, vol. 14, no. 2, pp. 240–250, Feb. 2020.

[31] M. Mlynczak, T. A. Valdez, and W. Kukwa, "Joint apnea and body position analysis for home sleep studies using a wireless audio and motion sensor," *IEEE Access*, vol. 8, pp. 170579–170587, 2020.